Abdulaziz AL-FADHLI [1], Khalid ALGHANIM [2],
Emad KHORSHID [2]

A shaped input emergency braking with safety limits for crane systems

This research presents an innovative braking strategy that integrates advanced input shaping techniques with dual-input methodology, incorporating both polynomial and step inputs. Through rigorous analytical analysis, the study determines optimal braking parameters and control input configurations to effectively eliminate oscillations and residual vibrations during post-braking operations. The developed model demonstrates significant improvements in braking performance by incorporating payload swing dynamics, while simultaneously achieving reduced braking times. Experimental validation substantiates the numerical predictions, confirming the efficacy of the proposed strategy. The strong correlation between analytical forecasts and experimental outcomes validates the model's accuracy and reliability. This research establishes a comprehensive methodology for enhancing overhead crane braking capabilities, offering substantial potential for improving both safety standards and operational efficiency in industrial applications.

1. Introduction

Cranes play a vital role in handling cargo and heavy loads across ports, construction sites, and industrial sectors, including automotive manufacturing. A significant challenge in crane operations is managing payload swing at the destination point, which substantially increases transfer time between positions. As underactuated nonlinear mechanical systems, cranes face inherent difficulties in

✉ Emad KHORSHID, e-mail: emad.korshid@ku.edu.kw

[1] Automotive & Marine Engineering Department, College of Technological Studies, Public Authority for Applied Education and Training (PAAET), Shuwaikh, Kuwait

[2] Department of Mechanical Engineering, College of Engineering and Petroleum, Kuwait University, Safat, Kuwait

mitigating payload vibration during operation. This challenge is particularly pronounced in overhead crane systems, which, despite their underactuated nature, are predominantly operated manually, requiring exceptional skill from operators. The development of automated control strategies has become crucial to addressing the limitations of manual operation, including inefficiency and reduced precision. Fundamentally, effective crane control aims to enable rapid point-to-point transfers while suppressing payload swing and maintaining operator safety [1].

A thorough examination of crane control strategies revealed that the majority of research is focused on limiting payload swing during operation [1–3]. Ramli's review classified the crane control solution into two primary control schools: the first one is the feedback control methods [4, 5], and the second one is the open-loop control methods [6, 7]. There is a combination of the previous two controllers which is called a hybrid control [8–11].

Feedback control methods for load oscillation suppression with enhanced robustness against disturbances and parameter variations require precise state measurement of the system, as demonstrated in [12] and [13]. Kim and Lee [12], who established the efficacy of model-based Proportional, Integral, and Derivative (PID) control for container crane stabilization. The literature presents extensive research on crane feedback control methodologies [14–19]. Linear Quadratic Regulator (LQR) represents another significant feedback control approach, with multiple studies validating its effectiveness in crane systems [20–23]. However, a critical limitation in crane feedback control research is the frequent oversight of human operator involvement. Since the operator functions as an additional feedback controller, his/her interaction can potentially degrade system performance [24]. Furthermore, feedback control methods face challenges in implementation due to requirements for increased system complexity and precise payload swing angle measurement [25]. These factors can lead to reduced controller effectiveness and potential system instability. Additionally, closed-loop control systems suffer from inherent limitations in response time due to feedback loop input delays [26, 27].

Feedforward methods in crane systems suppress payload vibrations during loading-unloading maneuvers through precise shaping of actuator commands. Input shaping, a particularly effective technique for vibration reduction in underactuated systems, operates by convolving a sequence of impulses with a reference command to generate a unified shaped command that effectively mitigates payload vibrations [28]. Vaughan et al. [25] demonstrated the superiority of command shaping over feedback control in crane applications. Extensive research has validated that anti-swing crane control implementing input shaping achieves significant payload swing reduction while maintaining minimal time delay [29–35]. The spectrum of input shaping methods includes zero vibration (ZV) and zero-vibration derivative (ZVD) techniques for overhead cranes [36–38], and extends to more sophisticated approaches such as zero vibration derivative-derivative-derivative (ZVDDD) specifically designed for liquid cargo applications [39]. However, while these shapers effectively eliminate residual vibrations, they introduce significant

actuator jerks that accelerate motor wear, resulting in increased operational and maintenance costs [38, 40, 41].

Research efforts in crane systems have predominantly focused on transportation tasks, where the primary challenge lies in achieving precise trolley positioning while eliminating payload swing. However, there is a pressing need to develop control methods that prioritize operational safety. Overhead crane systems typically operate in confined spaces occupied by personnel and other cargo, creating significant risk factors. In hazardous environments or crowded locations, accidental collisions between the payload and workers or surrounding cargo could result in severe financial losses or fatalities. Despite these critical safety concerns, the literature reveals a notable scarcity of research addressing safety-oriented control methods for crane systems. One of the early works on crane braking control is done by Yamamoto et al. [42]. The researchers developed an anti-sway control method specifically designed for emergency stops, based on the inverse dynamics of the crane mechanism. Their approach integrates real-time obstacle detection with inverse dynamics calculations to enable effective emergency stop control. The methodology was validated through experimental demonstrations, implementing a two-stage switching control strategy that independently addresses swing suppression and trolley braking objectives [43]. The switching timing between the two controllers is precisely determined through rigorous mathematical analysis to ensure optimal balance between safety and efficiency requirements. While experimental and computational results confirm the effectiveness of the proposed braking control method, a notable limitation emerges: the inability to achieve both objectives simultaneously results in significant payload swing during trolley braking operations. Chen et al. [44] proposed a fuzzy logic-based braking method to simultaneously achieve trolley braking and swing suppression objectives. Their approach incorporated trajectory planning techniques for known obstacle avoidance. However, a significant limitation of this research lies in the absence of theoretical guarantees for the proposed fuzzy controllers' performance. The study also addressed bridge crane safety considerations through the integration of online physical state monitoring and control models [44]. The researchers identified that safe braking distance must be variable to account for payload swing dynamics. In response, they developed a Model Predictive Control (MPC)-based anti-swing method that accommodates non-zero initial states. This approach guides the crane along a reference trajectory toward a stable stop state while suppressing swing oscillations through an optimized cost function and modified reference trajectory. The MPC braking control system incorporates an offline learning mechanism to establish a statistical correlation between crane velocity and safe braking distance. Both simulation studies and physical crane experiments validated the effectiveness of their safe braking distance prediction methodology for bridge crane control.

The integration of swing suppression proved crucial for ensuring safe braking operations [45]. This research leverages the coupling behavior between trolley motion and swing angles to develop enhanced coupling terms, derived through detailed

analysis of crane dynamics and swing suppression requirements. These coupling terms are integrated with the crane's mechanical energy function to incorporate swing angle feedback and improve oscillation damping. Safety considerations are addressed through the implementation of barrier function-like terms that constrain payload and hook horizontal positions within permissible boundaries. The resulting swing-suppression-guaranteed braking method is developed with a comprehensive mathematical analysis to validate its performance characteristics. Experimental validation is conducted using a hardware crane testbed to demonstrate the method's practical effectiveness.

Previous research in crane safety control has primarily focused on emergency braking and obstacle avoidance, notably without incorporating input shaping control techniques. Emergency braking for cranes presents an inherent conflict: the need for rapid trolley deceleration directly contradicts the goal of minimizing payload swing angles, as aggressive braking inevitably induces significant oscillations. To address this fundamental challenge, this study investigates the application of various input shapers for load swing suppression during emergency braking scenarios. The proposed methodology employs a two-stage approach, with the initial stage utilizing time-optimal rigid-body motion (TORB) to achieve trolley deceleration at maximum allowable acceleration rates [46]. This approach ensures minimal braking distance for optimal safety performance. However, the initial stage's braking scheme generates significant swing oscillations at motion termination, necessitating a second stage for oscillation suppression. In this subsequent phase, the trolley is actuated in the opposite direction of the desired location using specialized input shaping techniques [47]. These methods are designed to eliminate the payload swing. This research presents several key contributions through its novel braking strategy, which employs input shaping methodology to eliminate hazardous residual payload vibrations. The proposed approach significantly improves braking performance by simultaneously reducing both stopping distance and braking duration. Furthermore, the method implements sophisticated optimization techniques for the shaped input, utilizing additional independent variables to achieve more efficient and refined braking control.

2. Mathematical model

A standard overhead crane model comprises a lumped mass payload suspended by a fixed-length cable from a massless trolley moving along the horizontal plane. The payload exhibits pendulum-like motion in the XY-plane, as illustrated in Fig. 1. The system's operation begins with an acceleration phase, during which the trolley receives a smooth second-degree polynomial acceleration input. This polynomial function implements a Zero Vibration (ZV) shaper, with coefficients defined in [48]. Following the acceleration phase, the system transitions to a cruising stage characterized by constant trolley velocity and stabilized payload motion.
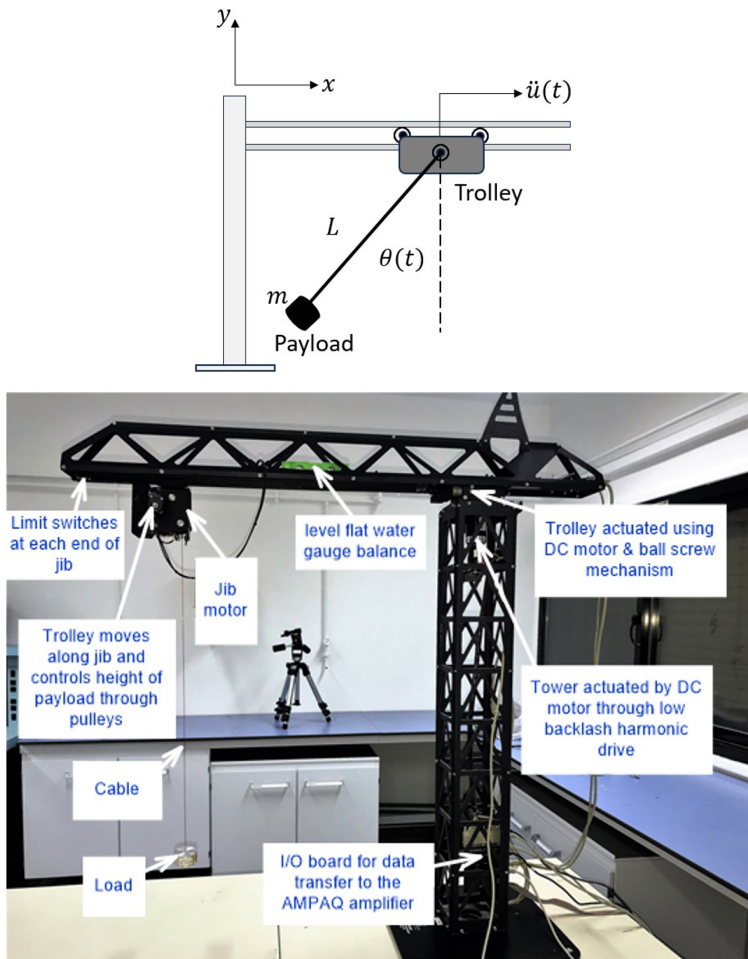
Fig. 1. Overhead crane model with the experimental setup

At this stage, the system initiates an emergency braking sequence. The braking strategy employs maximum deceleration capacity to minimize the payload's forward travel distance, followed by the application of a shaped input to bring the system to rest while eliminating sway motion. A critical constraint requires that all motion adjustments through the shaped input must occur within the maximum distance reached by the payload. Both trolley and payload must achieve zero vibration state within this prescribed braking distance, without exceeding it. The dynamics of this system can be described using the widely established overhead crane model, whose linear equation of motion is:

$$\ddot{\theta} + \omega^2\theta = \ddot{u}(t)/L, \tag{1}$$

$$\omega^2 = g/L, \tag{2}$$

where θ and $\ddot{\theta}$ are the swing angle and angular acceleration of the payload, respectively. ω is the natural frequency, $\ddot{u}$ is the input acceleration function to the trolley, L is the constant cable length, and g is the gravity constant. The proposed braking strategy will be examined by two different input functions: step-input and polynomial-input.

2.1. Step-input function

In this case, the input function is discretized into multiple Heaviside input steps. The first input step is the trolley's full deceleration capacity of duration t_d, which represents the braking stage, whereas the latter steps are of constant duration Δt, and applied to adjust the residual vibration and to brings the trolley to the rest, which is the shaping stage. Thus, the proposed step-input function is given by

$$\ddot{u}(t) = \begin{bmatrix} -\ddot{u}_{\max} & \ddot{u}_1 & \ddot{u}_2 & \cdots & \ddot{u}_N \end{bmatrix}^{\mathrm{T}}, \tag{3}$$

where $\ddot{u}_{\max}$ is the maximum acceleration of the trolley and N is the number of steps at the shaping stage. Assuming a small swing angle and using a convolution method yields to system response

$$\theta(t) = \frac{1}{L\omega} \int_0^t \ddot{u}(\tau) \sin\left(\omega(t - \tau)\right) \mathrm{d}\tau \tag{4}$$

Substituting Eq. (3) into Eq. (4) yields,

$$\theta(t) = \frac{\ddot{u}_{\max}}{g}(\cos \omega t - 1), \qquad 0 \leqslant t \leqslant t_d, \tag{5a}$$

$$\dot{\theta}(t) = -\frac{\omega \ddot{u}_{\max}}{g}\sin \omega t, \qquad 0 \leqslant t \leqslant t_d; \tag{5b}$$

$$\theta(t) = \frac{\ddot{u}_{\max}}{g}(\cos \omega t - 1) + \frac{1}{g}\sum_{k=1}^{n} \ddot{u}_k\Big(\cos\left(\omega(t - t_d - k\Delta t)\right) \\ - \cos\left(\omega(t - t_d - (k-1)\Delta t)\right)\Big), \tag{6a}$$

$$\dot{\theta}(t) = -\frac{\omega \ddot{u}_{\max}}{g}\sin \omega t + \frac{\omega}{g}\sum_{k=1}^{n} \ddot{u}_k\Big(-\sin\left(\omega(t - t_d - k\Delta t)\right) \\ + \sin\left(\omega(t - t_d - (k-1)\Delta t)\right)\Big), \tag{6b}$$

$$t_d + (n-1)\Delta t \leqslant t \leqslant t_d + n\Delta t, \quad n = 1, 2, 3, \ldots, N.$$

Integrating Eq. (3) with respect to time gives trolley velocity

$$\dot{u}(t) = v_c - \ddot{u}_{\max}t, \qquad 0 \leqslant t \leqslant t_d, \tag{7a}$$

$$\dot{u}(t) = v_c - (\ddot{u}_{\max} + \ddot{u}_n)\,t_d + \ddot{u}_n(t - n\Delta t) + \Delta t \sum_{k=1}^{n} \ddot{u}_k \tag{7b}$$

$$t_d + (n - 1)\Delta t \leqslant t \leqslant t_d + n\Delta t, \qquad n = 1, 2, 3, \ldots, N,$$

where v_c is the trolley constant velocity at the cruising stage.

Integrating Eq. (7) with respect to time gives trolley displacement starting from braking instance

$$u(t) = v_c t - \frac{1}{2}\ddot{u}_{\max}t^2, \qquad 0 \leqslant t \leqslant t_d, \tag{8a}$$

$$u(t) = \left(v_c - (\ddot{u}_{\max} + \ddot{u}_n)\,t_d + \Delta t \sum_{k=1}^{n} \ddot{u}_k\right)t + \frac{1}{2}\ddot{u}_n(t - n\Delta t)^2, \tag{8b}$$

$$t_d + (n - 1)\Delta t \leqslant t \leqslant t_d + n\Delta t, \quad n = 1, 2, 3, \ldots, N.$$

Payload displacement x_p is given by

$$x_p(t) = u(t) - L\theta(t). \tag{9}$$

Hence, the payload displacement and velocity at the braking stage is

$$x_p(t) = v_c t - \frac{1}{2}\ddot{u}_{\max}t^2 - L\frac{\ddot{u}_{\max}}{g}(\cos \omega t - 1), \qquad 0 \leqslant t \leqslant t_d, \tag{10a}$$

$$\dot{x}_p(t) = v_c - \ddot{u}_{\max}t + \frac{\ddot{u}_{\max}}{\omega}\sin \omega t, \qquad 0 \leqslant t \leqslant t_d. \tag{10b}$$

The farthest displacement of the payload at the braking stage is at zero payload velocity. Therefore, equating Eq. (10b) to zero gives the braking time t_d

$$\alpha - \sin \alpha = \frac{\omega v_c}{\ddot{u}_{\max}}, \qquad t_d = \frac{\alpha}{\omega}. \tag{11}$$

Eq. (11) is a nonlinear equation; therefore, a numerical method will be used to solve for α. In order to have zero vibration at the end of the maneuver and to bring the system to the rest, Eqs. (6) and (7b) are used and evaluated at the final time, $t_f = t_d + N\Delta t$, equated to zero, and solved for the step inputs $\ddot{u}_1$, $\ddot{u}_2$, ..., $\ddot{u}_N$

$$\sum_{k=1}^{N} \ddot{u}_k \left(\cos\left(\omega(N - k)\Delta t\right) - \cos\left(\omega(N - k + 1)\Delta t\right)\right) = \ddot{u}_{\max}\left(1 - \cos \omega t_f\right), \tag{12a}$$

$$\sum_{k=1}^{N} \ddot{u}_k \left(-\sin\left(\omega(N-k)\Delta t\right) + \sin\left(\omega(N-k+1)\Delta t\right)\right) = \ddot{u}_{\max}\sin\omega t_f, \quad (12b)$$

$$\Delta t \sum_{k=1}^{N} \ddot{u}_k = \ddot{u}_{\max} t_d - v_c. \quad (12c)$$

Eq. (12) can be arranged in a matrix form

$$
\begin{bmatrix} \beta_1 & \beta_2 & \cdots & \beta_N \\ \gamma_1 & \gamma_2 & \cdots & \gamma_N \\ 1 & 1 & \cdots & 1 \end{bmatrix}
\begin{bmatrix} \ddot{u}_1 \\ \vdots \\ \ddot{u}_N \end{bmatrix}
=
\begin{bmatrix} \ddot{u}_{\max}\left(1 - \cos\omega t_f\right) \\ \ddot{u}_{\max}\sin\omega t_f \\ \left(\ddot{u}_{\max}t_d - v_c\right)/\Delta t \end{bmatrix},
$$

$$\beta_k = \cos\left(\omega\left(N-k\right)\Delta t\right) - \cos\left(\omega\left(N-k+1\right)\Delta t\right),$$

$$\gamma_k = -\sin\left(\omega\left(N-k\right)\Delta t\right) + \sin\left(\omega\left(N-k+1\right)\Delta t\right),$$

$$k = 1, 2, 3, \ldots, N. \quad (13)$$

For $N > 3$, the system becomes an underdetermined system containing more unknowns ($\ddot{u}_k$) than the governing equations. Thus, Eq. (13) can be rearranged in

$$
\begin{bmatrix} \beta_1 & \beta_2 & \beta_3 \\ \gamma_1 & \gamma_2 & \gamma_3 \\ 1 & 1 & 1 \end{bmatrix}
\begin{bmatrix} \ddot{u}_1 \\ \ddot{u}_2 \\ \ddot{u}_3 \end{bmatrix}
+
\begin{bmatrix} \beta_4 & \beta_5 & \cdots & \beta_N \\ \gamma_4 & \gamma_5 & \cdots & \gamma_N \\ 1 & 1 & \cdots & 1 \end{bmatrix}
\begin{bmatrix} \ddot{u}_4 \\ \vdots \\ \ddot{u}_N \end{bmatrix}
=
\begin{bmatrix} \ddot{u}_{\max}\left(1 - \cos\omega t_f\right) \\ \ddot{u}_{\max}\sin\omega t_f \\ \left(\ddot{u}_{\max}t_d - v_c\right)/\Delta t \end{bmatrix}. \quad (14)
$$

The input steps ($\ddot{u}_4, \ldots, \ddot{u}_N$) are independent inputs that can be optimized according to the system objectives, whereas ($\ddot{u}_1, \ddot{u}_2, \ddot{u}_3$) are dependent inputs that determined by

$$
\begin{bmatrix} \ddot{u}_1 \\ \ddot{u}_2 \\ \ddot{u}_3 \end{bmatrix}
=
\begin{bmatrix} \beta_1 & \beta_2 & \beta_3 \\ \gamma_1 & \gamma_2 & \gamma_3 \\ 1 & 1 & 1 \end{bmatrix}^{-1}
\left(
\begin{bmatrix} \ddot{u}_{\max}\left(1 - \cos\omega t_f\right) \\ \ddot{u}_{\max}\sin\omega t_f \\ \left(\ddot{u}_{\max}t_d - v_c\right)/\Delta t \end{bmatrix}
-
\begin{bmatrix} \beta_4 & \beta_5 & \cdots & \beta_N \\ \gamma_4 & \gamma_5 & \cdots & \gamma_N \\ 1 & 1 & \cdots & 1 \end{bmatrix}
\begin{bmatrix} \ddot{u}_4 \\ \vdots \\ \ddot{u}_N \end{bmatrix}
\right). \quad (15)
$$

Eq. (15) gives the dependent input steps that satisfy system conditions and constraints. Nevertheless, in the case of $N = 3$, Eq. (15) is reduced in

$$
\begin{bmatrix} \ddot{u}_1 \\ \ddot{u}_2 \\ \ddot{u}_3 \end{bmatrix}
= \phi^{-1}
\begin{bmatrix} \ddot{u}_{\max}\left(1 - \cos\omega t_f\right) \\ \ddot{u}_{\max}\sin\omega t_f \\ \left(\ddot{u}_{\max}t_d - v_c\right)/\Delta t \end{bmatrix}, \qquad
\phi =
\begin{bmatrix} \beta_1 & \beta_2 & \beta_3 \\ \gamma_1 & \gamma_2 & \gamma_3 \\ 1 & 1 & 1 \end{bmatrix} \quad (16)
$$

in which the determinant $|\phi|$ governs the magnitude of the input steps. The special case $|\phi| \cong 0$ leads to tremendous acceleration magnitudes that should be avoided, and its corresponding duration time $t_f = 3\Delta t$ can be determined by

$$|\phi| = 16\sin\left(\omega t_f/3\right)\left(\sin\left(\omega t_f/6\right)\right)^4 = 0, \quad t_f = 3\pi/\omega, \ 6\pi/\omega, \ \ldots \quad (17)$$

Eq. (17) illustrates the shaping-stage maneuvering time that should be avoided.

2.2. Polynomial-input function

The system implements polynomial input functions of varying degrees, with the system response being substantially influenced by their smoothness and continuity characteristics. While the initial braking action continues to utilize the trolley's maximum deceleration capacity, this is followed by a shaped input acceleration phase designed to bring the system to rest with complete elimination of residual vibration. The shaped acceleration function is given by

$$
\ddot{u}(t) = \begin{cases} -\ddot{u}_{\max}, & 0 \leqslant t \leqslant t_d, \\ \displaystyle\sum_{k=1}^{N} c_k t^{k-1}, & t_d \leqslant t \leqslant t_f, \end{cases} \tag{18}
$$

where c_k are the polynomial constant coefficients. Substituting Eq. (18) into Eq. (1) and solving for payload angle yield,

$$
\theta(t) = \frac{\ddot{u}_{\max}}{g}(1 - \cos \omega t) + \frac{1}{L\omega} \int_{t_d}^{t} \left(\sum_{k=1}^{N} c_k t^{k-1} \right) \sin(\omega(t - \tau)) \, d\tau, \tag{19a}
$$

$$
\dot{\theta}(t) = \frac{\omega \ddot{u}_{\max}}{g} \sin \omega t + \frac{1}{L\omega} \frac{d}{dt} \int_{t_d}^{t} \left(\sum_{k=1}^{N} c_k t^{k-1} \right) \sin(\omega(t - \tau)) \, d\tau. \tag{19b}
$$

The integral term is exceedingly complicated but can be obtained in exact enormous form. It has been determined and implemented by MATLAB. The exact form is found by a recursive integration technique depending on the degree of the polynomial. Trolley velocity and displacement are measured just after applying the brakes, and can be determined by integrating Eq. (18) with respect to time

$$
\dot{u}(t) = \begin{cases} v_c - \ddot{u}_{\max} t, & 0 \leqslant t \leqslant t_d, \\ \displaystyle v_c - \ddot{u}_{\max} t_d + \sum_{k=1}^{N} c_k \left(t^k - t_d^k \right), & t_d \leqslant t \leqslant t_f, \end{cases} \tag{20}
$$

$$
u(t) = \begin{cases} v_c t - \dfrac{1}{2} \ddot{u}_{\max} t^2, & 0 \leqslant t \leqslant t_d, \\ \displaystyle v_c t_d - \dfrac{1}{2} \ddot{u}_{\max} t_d^2 + \sum_{k=1}^{N} \frac{c_k}{k(k+1)} \left(t^{k+1} - t_d^{k+1} \right), & t_d \leqslant t \leqslant t_f. \end{cases} \tag{21}
$$

Braking time t_d is determined by Eq. (11). Evaluating Eqs. (19) and (20) at the final time t_f and equating to zero yield

$$
\int_{t_d}^{t_f} \left(\sum_{k=1}^{N} c_k t^{k-1} \right) \sin(\omega(t - \tau)) \, d\tau = \frac{\ddot{u}_{\max}}{\omega} \left(\cos \omega t_f - 1 \right), \tag{22a}
$$

$$\left[\frac{d}{dt}\int_{t_d}^{t}\left(\sum_{k=1}^{N}c_k t^{k-1}\right)\sin\left(\omega(t-\tau)\right)d\tau\right]_{t=t_f} = -\ddot{u}_{max}\sin\omega t_f, \qquad (22b)$$

$$\sum_{k=1}^{N}c_k\left(t_f^k - t_d^k\right)/k = \ddot{u}_{max}t_d - v_c. \qquad (22c)$$

Rearranging Eq. (22) in a matrix form

$$\begin{bmatrix}\psi_1 & \psi_2 & \psi_3\\ \lambda_1 & \lambda_2 & \lambda_3\\ \delta_1 & \delta_2 & \delta_3\end{bmatrix}\begin{bmatrix}c_1\\ c_2\\ c_3\end{bmatrix} + \begin{bmatrix}\psi_4 & \psi_5 & \cdots & \psi_N\\ \lambda_4 & \lambda_5 & \cdots & \lambda_N\\ \delta_4 & \delta_5 & \cdots & \delta_N\end{bmatrix}\begin{bmatrix}c_4\\ \vdots\\ c_N\end{bmatrix} = \begin{bmatrix}\ddot{u}_{max}\left(\cos\omega t_f - 1\right)/\omega\\ -\ddot{u}_{max}\sin\omega t_f\\ \ddot{u}_{max}t_d - v_c\end{bmatrix},$$

$$\psi_k = \int_{t_d}^{t_f}t^{k-1}\sin\left(\omega(t-\tau)\right)d\tau, \quad \lambda_k = \left[\frac{d}{dt}\int_{t_d}^{t}t^{k-1}\sin\left(\omega(t-\tau)\right)d\tau\right]_{t=t_f}, \qquad (23)$$

$$\delta_k = \left(t_f^{k+1} - t_d^{k+1}\right)/k.$$

Substituting the independent (optimizing) coefficients (c_4, ..., c_N) into Eq. (23) and solving for the dependent coefficients (c_1, c_2, c_3) give the input-polynomial coefficients. In the case of $N = 3$, Eq. (23) is reduced to

$$\Omega\begin{bmatrix}c_1\\ c_2\\ c_3\end{bmatrix} = \begin{bmatrix}\ddot{u}_{max}\left(\cos\omega t_f - 1\right)/\omega\\ -\ddot{u}_{max}\sin\omega t_f\\ \ddot{u}_{max}t_d - v_c\end{bmatrix}, \qquad \Omega = \begin{bmatrix}\psi_1 & \psi_2 & \psi_3\\ \lambda_1 & \lambda_2 & \lambda_3\\ \delta_1 & \delta_2 & \delta_3\end{bmatrix}, \qquad (24)$$

where the determinant $|\Omega|$ regulates the magnitude of the coefficients (c_1, c_2, c_3). Excessively large polynomial coefficients correspond to zero determinant

$$|\Omega| = 4t_f\left(1 - \omega^2 t_f^2/3\right)\cos\left(\omega t_f\right) + \omega t_f^2\left(4 - \omega^2 t_f^2/6\right)\sin\left(\omega t_f\right)$$
$$- 2\omega^2 t_f^3/3 - 4t_f = 0. \qquad (25)$$

Eq. (25) can be solved numerically to obtain the multiple extreme final times (t_f) that should be avoided.

Both proposed input functions successfully satisfy the system's final conditions using a minimum of three inputs – whether implemented through three steps in the Heaviside function or three terms in the polynomial input. While this minimum configuration leaves no room for optimization, introducing additional inputs to the shaped input function creates independent variables that enable optimization. This optimization process focuses specifically on minimizing the maximum payload displacement that occurs during braking operations. Constant acceleration

necessitates changes in velocity, resulting in variable power requirements. When operating at full electrical capacity, the motor generates increasing trolley velocity and consequently, variable mechanical power. While utilizing the motor's maximum capacity ensures optimal time to reach the desired trolley speed, perfectly constant acceleration cannot be guaranteed. Rather, a steady increase in trolley velocity is achieved through motor input current regulation, approximating constant acceleration.

3. Results and discussions

The research methodology encompassed both numerical simulation and experimental validation of various functions and parameters. Experimental verification was conducted using a 3-degrees-of-freedom Quanser tower crane system. The setup features two DC motors for lifting operations, controlled through a PID controller implemented on a MATLAB/Simulink real-time system. Precision positioning of the crane's trolley and payload is achieved through optical encoders mounted on each DC motor, providing 1024 points per revolution resolution. The system operates within performance parameters of 0.27 m/s maximum velocity and 0.9 m/s^2 maximum acceleration for trolley movement.

The analysis incorporated multiple input functions: Heaviside functions with 3, 4, and 5 steps, and polynomial functions of degrees 2, 3, and 4. A key finding revealed that second-degree polynomials and 3-step functions contain no independent optimization terms, but rather three dependent terms that satisfy the system's final conditions. The 3-degree polynomial and 4-step functions each provide a single independent term for input optimization, while 4-degree polynomials and 5-step functions offer two independent terms for solution optimization. Notably, viable solutions could not be achieved with either second-degree polynomials or three-step functions without resorting to impractically long maneuver times.

Minor discrepancies between theoretical predictions and experimental measurements were observed. These variations can be attributed to multiple experimental factors that were difficult to control precisely, including: uncertainties in mass and length measurements, cable elasticity effects, non-uniform payload mass distribution, payload rotational inertia, inherent friction within the experimental setup, and various other secondary factors.

Fig. 2 presents a comparative analysis of payload angle trajectories over time for various input acceleration functions: third and fourth-degree polynomials, and 4-step and 5-step Heaviside functions. Both theoretical (T) and experimental (E) results are shown for cable lengths of 0.2 m and 0.5 m. The system demonstrates faster braking times with a shorter cable length due to its higher natural frequency and reduced periodic time, enabling more rapid control response.

Fig. 3 illustrates the theoretical and experimental trolley velocity profiles for cable lengths of 0.2 m and 0.5 m. Polynomial input functions, while requiring longer maneuver times compared to Heaviside functions, generate significantly
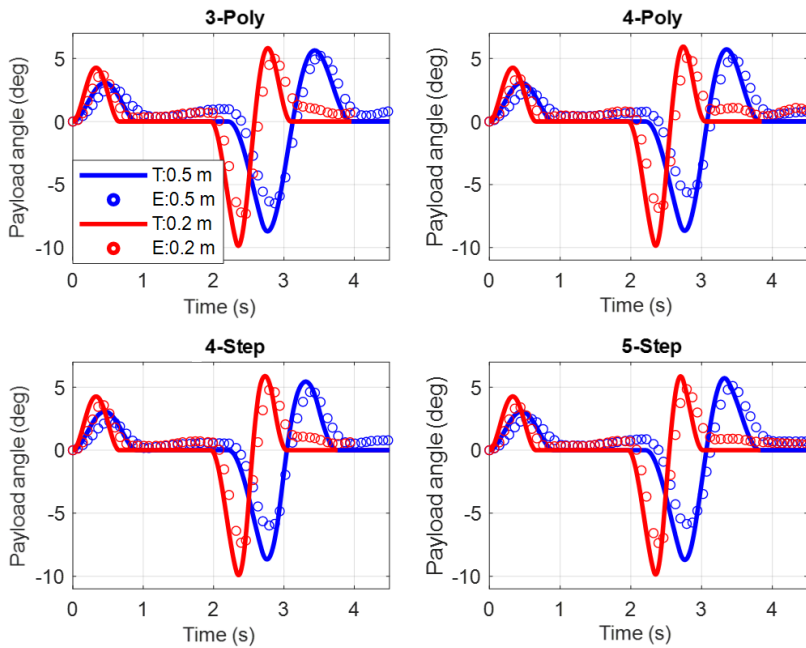
Fig. 2. Payload angle vs. time of different input functions and cable lengths
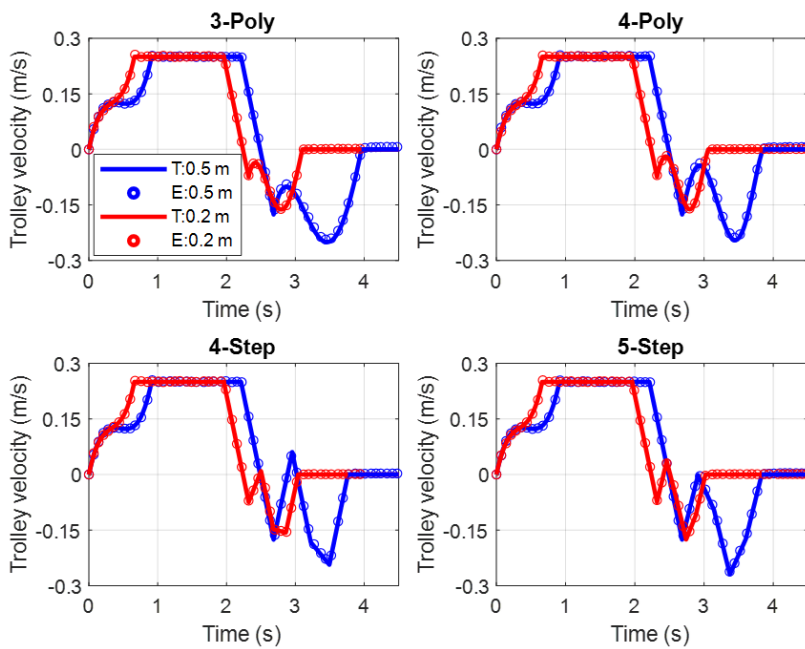

Fig. 3. Trolley velocity vs. time of different input functions and cable lengths

smoother motion profiles, making them advantageous for applications requiring smooth operation. Fig. 4 demonstrates the increased jerk characteristics associated with step-input functions, particularly pronounced when higher numbers of input steps are required. This jerky motion makes step-input functions less suitable for motor control applications. In contrast, polynomial functions maintain consistent smoothness throughout the maneuver, with the notable exception of the initial braking phase, where an unavoidable discontinuity occurs in the input function due to the brake application.
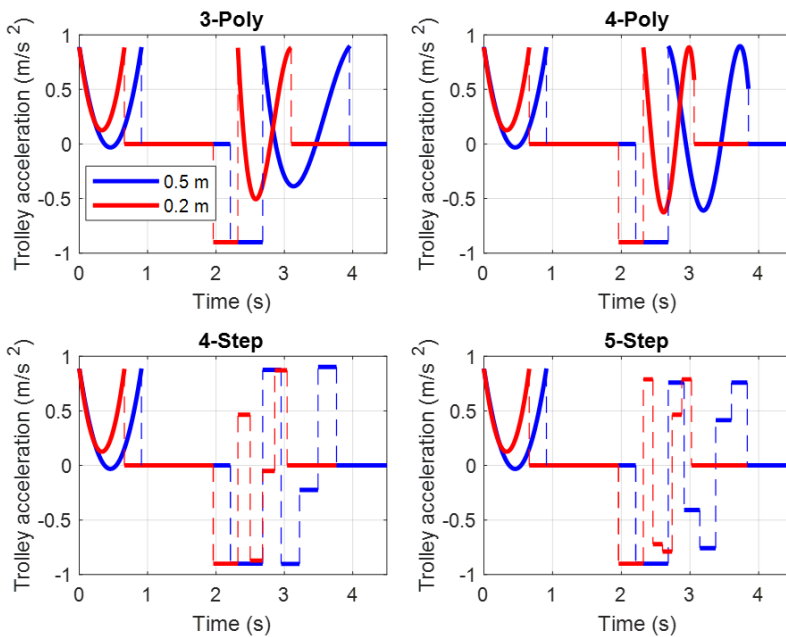
Fig. 4. Trolley acceleration vs. time of different input functions and cable lengths

Fig. 5 demonstrates the displacement profiles for both trolley (T) and payload (P) at cable lengths of 0.5 m and 0.2 m. During the cruising stage, trolley and payload motions coincide, characterized by constant velocity and absence of oscillation. Upon entering the braking stage, the payload exhibits greater forward displacement due to pendulum-like swing motion. The system ultimately achieves a complete rest state, with both trolley and payload coming to a stop at the conclusion of the maneuver.

Fig. 6 presents a comparative analysis between the proposed and classical input shapers for a cable length of 0.5 m, illustrating theoretical payload angle and displacement trajectories versus time following brake application. The comparison encompasses the proposed third-degree polynomial and 4-step functions against classical Time-Optimal Rigid-Body (TORB) and Zero Vibration (ZV) shapers. Payload displacement measurements commence from the braking initiation point.
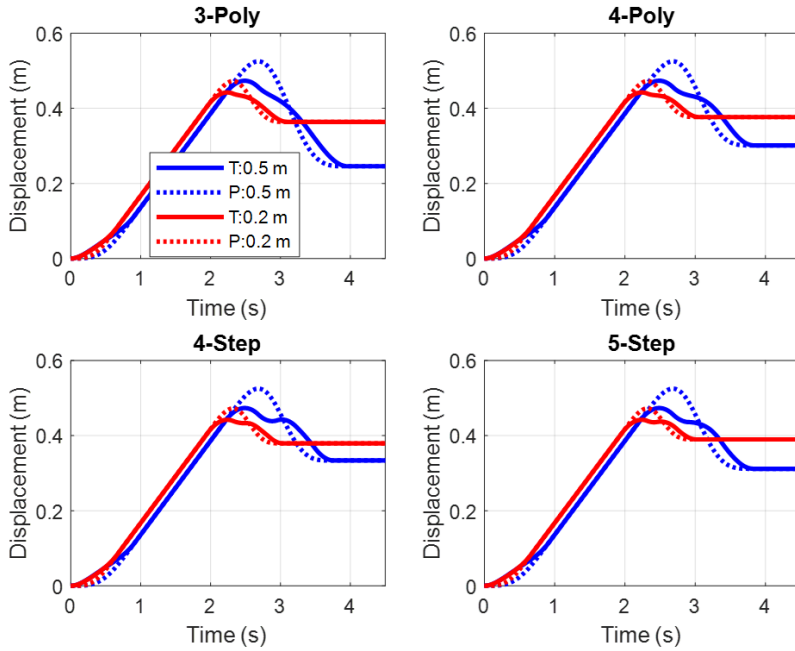
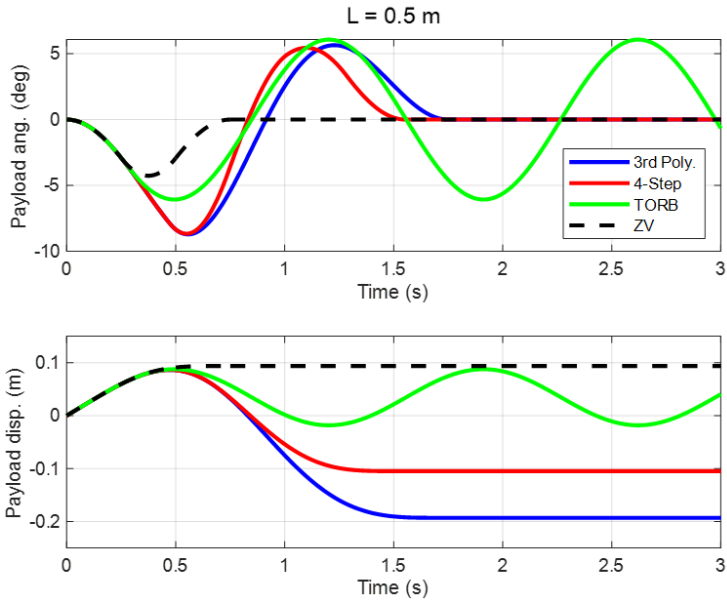Fig. 5. Trolley and payload displacement vs. time of different input functions and cable lengths

Fig. 6. Payload angle and displacement vs. time of different shapers

The proposed strategy successfully eliminates residual vibration while maintaining a safe displacement margin at maneuver completion. Furthermore, it achieves reduced maximum payload displacement compared to both classical approaches – 1.4% less than the TORB shaper and 7.8% less than the ZV shaper. Notably, unlike the TORB shaper, the proposed strategy eliminates residual vibration.

While the classical Zero-Vibration (ZV) shaper effectively eliminates system vibration, it results in maximum payload displacement. The Time-Optimal Rigid Body (TORB) input achieves reduced displacement but exhibits oscillatory payload behavior. The proposed shaping method synthesizes the advantages of both approaches, simultaneously minimizing settling displacement and enhancing post-braking system stability. This performance is further improved through the implementation of additional terms in the optimized input function.

Fig. 7 provides a comprehensive comparison between the proposed braking strategy and classical approaches (TORB and ZV shapers) during the braking stage. Fig. 7a illustrates braking action completion times, while Figs. 7b, 7c, and 7d present payload maximum displacement, payload swing amplitude, and terminal trolley speed, respectively. The ZV shaper requires extended duration to achieve swing suppression before complete stoppage. The proposed strategy achieves faster system braking prior to the shaping stage, whereas the TORB shaper, despite its rapid braking time, results in persistent oscillations. Notably, the proposed strategy achieves the smallest maximum payload displacement among all shapers, max-
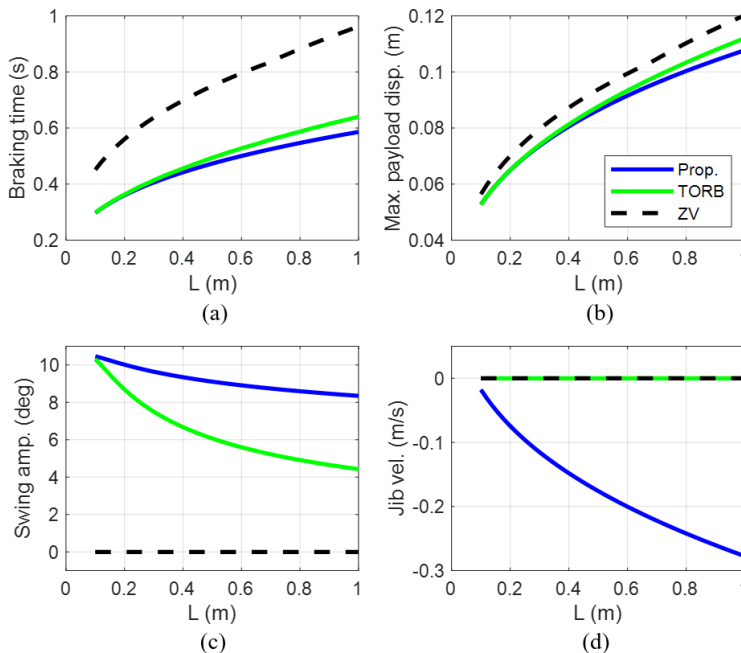

Fig. 7. Cable length of different shapers vs: (a) brake time, (b) payload displacement, (c) payload vibration amplitude, (d) trolley velocity

imizing obstacle avoidance capability. Although the proposed approach exhibits peak swing amplitude at braking completion, this oscillation is subsequently eliminated during the shaping stage. The strategy's negative trolley velocity at braking completion contributes to enhanced braking performance.

Fig. 8 depicts the relationship between maximum input acceleration and shaping time for various functions at cable lengths of 0.2 m and 0.5 m. The analysis reveals that vertical asymptotes in maximum acceleration patterns decrease both with increasing cable length and when using Heaviside functions. The exceptionally high acceleration values correspond to mathematical singularities where the matrix determinant approaches zero in Eqs. (17) and (25). These regions of zero or near-zero determinants must be avoided during shaper function design. The diversity of zero-determinant regions across different shaping functions provides greater flexibility in function selection. Additionally, increasing either the polynomial degree or the number of steps expands the optimization space, resulting in fewer vertical asymptotes of high acceleration values.
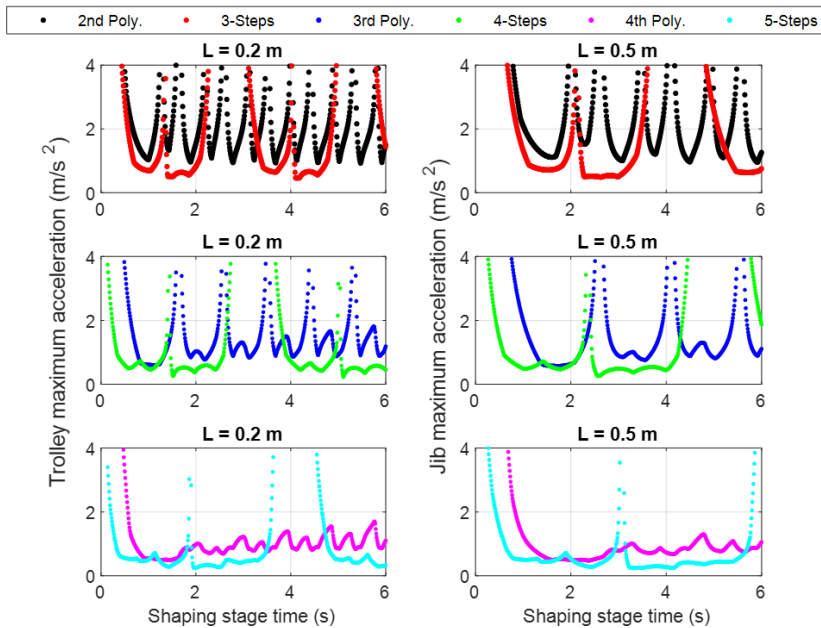
Fig. 8. Trolley maximum acceleration vs. shaping-stage time of different functions and lengths

Fig. 9 shows the maximum trolley acceleration versus shaping-stage time of the 3-step and second-degree polynomial functions for cable length of 0.5 m (ω = 4.43 rad/s). The 3-step function shows asymptotes at the singular values t_f = 2.13, 4.26 s, according to Eq. (17). The second-degree polynomial function shows its asymptotes according to the solution of Eq. (25) at t_f = 2.03, 2.60, 3.49, 4.11, 4.92, 5.56 s, and the plot of the determinant $|\Omega|$ passes through its

roots at these values. The Heaviside function demonstrates superior performance characteristics compared to the polynomial function due to its reduced number of mathematical singularities, making it more robust for practical implementation.
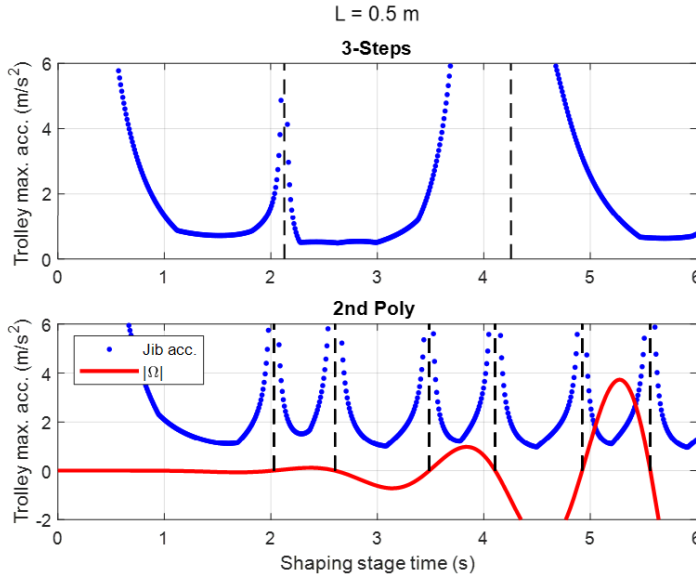

Fig. 9. Trolley maximum acceleration and $|\Omega|$ vs. shaping-stage time of different functions

4. Conclusions

This study presents compelling evidence for the efficacy of a novel braking strategy in overhead crane systems through the integration of sophisticated input shaping techniques with optimized polynomial and step inputs. Rigorous analytical analysis has successfully identified optimal control input configurations that effectively suppress both oscillations during braking and residual vibrations in the post-braking phase. The proposed methodology achieves a critical balance between competing objectives: minimizing payload swing while reducing overall braking time.

Experimental validation has demonstrated remarkable concordance with theoretical predictions, confirming the mathematical model's accuracy and reliability. The strategy's success in reducing maximum payload displacement compared to conventional approaches-specifically showing improvements of 1.4% over TORB and 7.8% over ZV shapers-highlights its practical significance. Furthermore, the methodology's ability to eliminate residual vibrations while maintaining shorter braking times represents a substantial advancement over existing techniques.

The practical implications of this research extend beyond theoretical contributions, offering tangible benefits for industrial applications. The strategy's capacity

to enhance both safety and operational efficiency addresses critical challenges in industrial environments where overhead cranes operate in confined spaces with personnel and valuable cargo. The methodology's adaptability to different cable lengths and operating conditions further demonstrates its robust practical utility.

This research establishes a foundation for future developments in crane control systems, particularly in applications requiring precise maneuvering and rapid emergency responses. The successful implementation of this braking strategy represents a significant step toward improving industrial safety standards while optimizing operational efficiency in overhead crane applications.

References

[1] R. Neitzel, N.S. Seixas, and K.K. Ren. A review of crane safety in the construction industry. *Applied Occupational and Environmental Hygiene*, 16(12):1106–1117, 2001. doi: 10.1080/10473220127411.

[2] W. Singhose, L. Porter, M. Kenison, and E. Kriikku. Effects of hoisting on the input shaping control of gantry cranes. *Control Engineering Practice*, 8(10):1159–1165, 2000. doi: 10.1016/S0967-0661(00)00054-X.

[3] L. Ramli, Z. Mohamed, A.M. Abdullahi, H.I. Jaafar, and I.M. Lazim. Control strategies for crane systems: A comprehensive review. *Mechanical Systems and Signal Processing*. 95:1–23, 2017. doi: 10.1016/j.ymssp.2017.03.015.

[4] M.I. Solihin, Wahyudi, and A. Legowo. Fuzzy-tuned PID anti-swing control of automatic gantry crane. *Journal of Vibration and Control*, 16(1):127–145, 2010. doi: 10.1177/1077546309103421.

[5] N. Sun, Y. Fang, and X. Zhang. Energy coupling output feedback control of 4-DOF underactuated cranes with saturated inputs. *Automatica*, 49(5):1318–1325, 2013. doi: 10.1016/j.automatica.2013.01.039.

[6] T. Singh. Jerk limited input shapers. *Journal of Dynamic Systems, Measurement, and Control*, 126(1):215–219, 2004. doi: 10.1115/1.1653808.

[7] W. Singhose. Command shaping for flexible systems: A review of the first 50 years. *International Journal of Precision Engineering and Manufacturing* ,10(4):153–168, 2009. doi: 10.1007/s12541-009-0084-2.

[8] S. Kapucu, G. Alici, and S. Bayseç. Residual swing/vibration reduction using a hybrid input shaping method. *Mechanism and Machine Theory*, 36(3):311–326, 2001. doi: 10.1016/S0094-114X(00)00048-3.

[9] Z.M. Chen, W.J. Meng, M.H. Zhao, and J.G. Zhang. Hybrid robust control for gantry crane system. *Applied Mechanics and Materials*, 29-32:2082–2088, 2010. doi: 10.4028/www.scientific.net/ AMM.29-32.2082.

[10] M. Hamdy, R. Shalaby, and M. Sallam. A hybrid partial feedback linearization and deadbeat control scheme for a nonlinear gantry crane, *Journal of the Franklin Institute*, 355(14):6286–6299, 2018. doi: 10.1016/j.jfranklin.2018.06.014.

[11] S.C. Duong, E. Uezato, H. Kinjo, and T. Yamamoto. A hybrid evolutionary algorithm for recurrent neural network control of a three-dimensional tower crane. *Automation in Construction*, 23:55–63, 2012. doi: 10.1016/j.autcon.2011.12.005.

[12] D.H. Kim and J.W. Lee, Model-based PID control of a crane spreader by four auxiliary cables. *Proceedings of the Institution of Mechanical Engineers, Part C: Journal of Mechanical Engineering Science*, 220(8):1151–1165, 2006. doi: 10.1243/09544062JMES120.

[13] H.M. Omar and A.H. Nayfeh. Anti-swing control of gantry and tower cranes using fuzzy and time-delayed feedback with friction compensation. *Shock and Vibration*, 12(2):73–89, 2005. doi: 10.1155/2005/890127.

[14] K. Kawada, H. Sogo, T. Yamamoto, and Y. Mada. Evolutionary computation in designing a robust PD sway controller for a mobile crane. In: *Proceedings of the International Conference on Control Applications*, vol. 2, pages 868–873, Glasgow, UK, 2002. doi: 10.1109/CCA.2002.1038716.

[15] M.I. Solihin, Wahyudi, M.A.S. Kamal, and A. Legowo. Objective function selection of GA-based PID control optimization for automatic gantry crane. In: *2008 International Conference on Computer and Communication Engineering*, pages 883–887, Kuala Lumpur, Malaysia, 2008. doi: 10.1109/ICCCE.2008.4580732.

[16] M.A. Ahmad, M.S. Ramli, M.A. Zawawi, and R.M. Raja Ismail. Hybrid collocated PD with non-collocated PID for sway control of a lab-scaled rotary crane. In: *2010 5th IEEE Conference on Industrial Electronics and Applications*, pages 707–711, Taichung, Taiwan 2010. doi: 10.1109/ICIEA.2010.5516968.

[17] J. Vaughan, A. Karajgikar, and W. Singhose. A study of crane operator performance comparing PD-control and input shaping. In: *Proceedings of the 2011 American Control Conference*, pages 545–550, San Francisco, CA, USA, 2011. doi: 10.1109/ACC.2011.5991506.

[18] C. Liu, H. Zhao, and Y. Cui. Research on application of fuzzy adaptive PID controller in bridge crane control system. In *2014 IEEE 5th International Conference on Software Engineering and Service Science*, pages 971–974, Beijing, China, 2014. doi: 10.1109/ICSESS.2014.6933727.

[19] H.I. Jaafar, S.Y.S. Hussien, R. Ghazali, and Z. Mohamed. Optimal tuning of PID+PD controller by PFS for gantry crane system. In: *2015 10th Asian Control Conference (ASCC)*, pages 1-6, Kota Kinabalu, Malaysia, 2015. doi: 10.1109/ASCC.2015.7244695.

[20] M.A. Ahmad, R.E. Samin, and M.A. Zawawi. Comparison of optimal and intelligent sway control for a lab-scale rotary crane system. In: *2010 Second International Conference on Computer Engineering and Applications*, pages 229–234, Bali, Indonesia, 2010. doi: 10.1109/ICCEA.2010.52.

[21] M.A. Ahmad, A.N. Nasir, R.M. Raja Ismail, and M.S. Ramli. Control schemes for input tracking and anti-sway control of a gantry crane. *Australian Journal of Basic and Applied Sciences*, 4(8):2280–2291, 2010.

[22] B. Yang and B. Xiong. Application of LQR techniques to the anti-sway controller of overhead crane. *Advanced Materials Research*, 139-141:1933–1936, 2010. doi: 10.4028/www.scientific.net/AMR.139-141.1933.

[23] J. Jafari, M. Ghazal, and M. Nazemizadeh. A LQR optimal method to control the position of an overhead crane. *International Journal of Robotics and Automation (IJRA)*, 3(4):252–258, 2014. doi: 10.11591/ijra.v3i4.6107.

[24] W. Singhose and D. Kim. Manipulation with tower cranes exhibiting double-pendulum oscillations. In: *Proceedings 2007 IEEE International Conference on Robotics and Automation*, pages 4550–4555, Rome, Italy, 2007. doi: 10.1109/ROBOT.2007.364180.

[25] J. Vaughan, E. Maleki, and W. Singhose. Advantages of using command shaping over feedback for crane control. In: *Proceedings of the 2010 American Control Conference*, pages 2308–2313, Baltimore, MD, USA, 2010. doi: 10.1109/ACC.2010.5530548.

[26] T.A. Sitompul. Human–machine interface for remote crane operation: A review. *Multimodal Technologies and Interaction*, 6(6):45, 2022. doi: 10.3390/mti6060045.

[27] H. Shi R. Li, X. Bai, Y. Zhang, L. Min, D. Wang, X. Lu, Y. Yan, and Y. Lei. A review for control theory and condition monitoring on construction robots. *Journal of Field Robotins*, 40(4):934–954, 2023. doi: 10.1002/rob.22156.

[28] W. Singhose, R. Eloundou, and J. Lawrence. Command generation for flexible systems by input shaping and command smoothing. *Journal of Guidance, Control, and Dynamics*, 33(6):1697–1707, 2010. doi: 10.2514/1.50270.

[29] M.J. Maghsoudi, Z. Mohamed, S. Sudin, S. Buyamin, H.I. Jaafar, and S.M. Ahmad. An improved input shaping design for an efficient sway control of a nonlinear 3D overhead crane with friction. *Mechanical Systems and Signal Processing*, 92:364–378, 2017. doi: 10.1016/j.ymssp.2017.01.036.

[30] D. Newman, S.-W. Hong, and J. E. Vaughan. The design of input shapers which eliminate nonzero initial conditions. *Journal of Dynamic Systems, Measurement and Control*, 140(10):101005, 2018. doi: 10.1115/1.4039668.

[31] P.P. Sahoo and W. Singhose. Effects of input shaping on impact loads during collisions involving flexible robots. In: *2018 IEEE 14th International Conference on Control and Automation (ICCA)*, pages 1004–1009, Anchorage, AK, USA, 2018. doi: 10.1109/ICCA.2018.8444309.

[32] J.J. Wilbanks, C.J. Adams, and M.J. Leamy. Two-scale command shaping for feedforward control of nonlinear systems. *Nonlinear Dynamics*, 92(3):885–903, 2018. doi: 10.1007/s11071-018-4098-0.

[33] H.I. Jaafar, Z. Mohamed, M.A. Shamsudin, N.A. Mohd Subha, L. Ramli, and A.M. Abdullahi. Model reference command shaping for vibration control of multimode flexible systems with application to a double-pendulum overhead crane. *Mechanical Systems and Signal Processing*, 115:677–695, 2019. doi: 10.1016/j.ymssp.2018.06.005.

[34] V.D. La and K.T. Nguyen. Combination of input shaping and radial spring-damper to reduce tridirectional vibration of crane payload. *Mechanical Systems and Signal Processing*, 116:310–321, 2019. doi: 10.1016/j.ymssp.2018.06.056.

[35] E. Khorshid, A. Al-Fadhli, K. Alghanim, and J. Baroon. Command shaping with reduced maneuvering time for crane control. *Journal of Vibration and Control*, 27(11-12):1311–1323, 2020. doi: 10.1177/1077546320940872.

[36] Y. Du, C. Wang, J. Lu, and Y. Zhou. Vibration suppression using multi-impulse robust shaping method of zero vibration and derivative. *Journal of Sound and Vibration*, 440:277–290, 2019. doi: 10.1016/j.jsv.2018.10.038.

[37] A. Wahrburg, J. Jurvanen, M. Niemelä, and M. Holmberg. On reference trajectory generation for overhead crane travel movements. *Automatisierungstechnik*, 70(3):300–311, 2022. doi: 10.1515/auto-2021-0147.

[38] K. Alghanim, A. Alfadhli, A. Alshehemah, and A. Mohammed. Crane systems performance optimization through harmonic input shaper. *International Journal of Dynamics and Control*, 12:1788–1800, 2023. doi: 10.1007/s40435-023-01321-3.

[39] W. Tian, J. Huang, and W. Singhose. Control of cooperative-transportation dynamics in twin-lift cranes suspending a liquid container. *IEEE Transactions on Industrial Electronics*, 71(4):4016–4025, 2024. doi: 10.1109/TIE.2023.3274868.

[40] A. Al-Fadhli and E. Khorshid. Payload oscillation control of tower crane using smooth command input. *Journal of Vibration and Control*, 29(3–4):902–915, 2023. doi: 10.1177/10775463211054640.

[41] N. Suksabai and I. Chuckpaiwong. The novel design of the command smoother for sway suppression of industrial overhead crane considering acceleration and deceleration limits. *International Journal of Dynamics and Control*, 11:2082–2100, 2023. doi: 10.1007/s40435-023-01156-y.

[42] M. Yamamoto, E. Honda, and A. Mohri. Safe automatic emergency stop control of gantry crane including moving obstacles in its workspace. In: *Proceedings of the 2005 IEEE International Conference on Robotics and Automation*, pages 253–258, Barcelona, Spain, 2005. doi: 10.1109/ROBOT.2005.1570128.

[43] B. Ma, Y. Fang, and Y. Zhang. Switching-based emergency braking control for an overhead crane system. *IET Control Theory & Applications*, 4(9):1739–1747, 2010. doi: 10.1049/iet-cta.2009.0277.

[44] H. Chen, G. Liu, G. Tian, J. Zhang, and Z. Ji. Safe distance prediction for braking control of bridge cranes considering anti-swing. *International Journal of Intelligent Systems*, 37(8):4845–4863, 2022. doi: 10.1002/int.22743.

[45] H. Chen, M. Li, and Y. Wu. An emergency braking method with swing suppression and safety limits consideration for double pendulum cranes. *Control Engineering Practice*, 139:105638, 2023. doi: 10.1016/j.conengprac.2023.105638.

[46] W. Singhose and L. Pao. A comparison of input shaping and time-optimal flexible-body control. *Control Engineering Practice*, 5(4):459–467, 1997. doi: 10.1016/S0967-0661(97)00025-7.

[47] K.A. Alhazza and Z.N. Masoud. A multi-mode smooth command shaper with an adjustable maneuver time. In: *Proceedings of the ASME 2015 Dynamic Systems and Control Conference*, vol. 3, paper V003T46A003,Columbus, Ohio, USA, 2015. doi: 10.1115/DSCC2015-9700.

[48] K.A. Alghanim, M.A. Majeed, and K.A. Alhazza. Adjustable-smooth polynomial command-shaping control with linear hoisting. *Journal of Vibration and Acoustics*, 140(6):061013, 2018. doi: 10.1115/1.4040236.